

Performance evaluation of a seawater exchange breakwater with Helmholtz resonator using OpenFOAM

Arun George^a and Il-Hyoung Cho^{*}

Department of Ocean System Engineering, Jeju National University, Jeju 690-756, Republic of Korea

(Received July 28, 2021, Revised August 12, 2021, Accepted August 17, 2021)

Abstract. In this study, the three dimensional numerical simulation of a seawater exchange breakwater using the Helmholtz resonator has been carried out in OpenFOAM. When the frequency of the incident wave coincides with one of the natural frequencies of a closed semi-circular resonator, resonance occurs in the resonator. The amplified water elevation in a resonator pushes the seawater periodically into the ocean/port side through the water channel and consequently improves the water quality of the port. The numerical model is based on Reynolds Averaged Navier Stokes equations with $k-\omega$ SST turbulence model. The VOF (Volume of Fluid) method is used to capture the free surface behavior. The numerical model is validated with model experiments conducted by Cho (2001) in a two-dimensional wave tank for regular waves. Numerical simulations for the prototype model in irregular waves based on the JONSWAP spectrum are also conducted to show whether the proposed seawater exchange breakwater can be feasible to the real seas. It is found that the seawater exchanging rate is greatly enhanced in the low-frequency wave region where the frequency of the Helmholtz resonance situates. If designing the Helmholtz resonator properly, it can supply the clean seawater sustainedly into the port side without additional electric power.

Keywords: CFD; Helmholtz resonator; irregular waves; seawater exchange breakwater; OpenFOAM®

1. Introduction

Breakwater is a man-made structure in a coastal zone that prohibits incident waves from entering the harbor to avoid excessive loading on mooring lines and fenders, hazards in cargo handling operations. The traditional gravity-type breakwaters, such as rubble mounds or concrete caisson structures (Van der Meer 1995), have shown a negative impact on marine ecosystems and pollution because of the reduction of water circulation in the partially closed ports and harbors. Currently, water quality in most ports and harbors has been extremely deteriorated, which not only adversely affects the ecosystem, but also has a severe odor. For this reason, when planning and designing the ports and harbors, a new concept of technology must be prepared to facilitate the exchange of seawater between the ocean and port side.

Most of the developed seawater exchange systems are normally effective only in the sea site of prevailed currents. A variety of studies have been done to propose the seawater exchange system that utilizes the wave power that exists abundantly in the ocean. The wave power can be maximized

*Corresponding author, Professor, E-mail: cho0904@jejunu.ac.kr

^a Ph.D. Student, E-mail: arunmvgeorge@gmail.com

when using resonance with the internal fluid in a closed structure. Lee (1995) presented a new type of caisson breakwater with a circular resonance channel with flow conduits to reduce wave overtopping and to accelerate the seawater exchange. However, this seawater exchange breakwater has a demerit in construction due to the complex geometry despite a good performance. Also, the construction cost increases tremendously with an inevitable increase of the caisson size for tuning the natural period of the circular channel with a period of incoming waves. Lee (2003) improved their design with a simpler L-shaped channel instead of a circular channel. Kim *et al.* (2011) applied the seawater exchange breakwater with an L-shaped water channel to the port of Jeju in South Korea and assessed the performance of the seawater exchange breakwater through the field test. They found the channel flow velocity in the order of 0.1 m/s can transport a large amount of the seawater into the port side.

The Helmholtz resonance used in the present study is sort of the resonance in a cavity, which is widely applied in fields of architectural acoustics, aircraft engines, and musical instruments. In the present study, the Helmholtz resonance is applied to develop a new-concept seawater exchange breakwater. To understand clearly the seawater exchange breakwater using the Helmholtz resonance, let's consider an array of semi-circular resonators with the entrance in line with a long and straight breakwater (see Fig. 1). Incident waves are partly reflected and partly absorbed along the breakwater. A small portion is diffracted through the entrance into the resonator and reflected repeatedly by the interior boundaries of the resonator. Some of the reflected wave energy escapes the resonator and radiates to the ocean again. If the incident wave frequency is close to the one of natural frequencies in the closed resonator, resonance will occur in the resonator so that a relatively weak incident wave can induce a large wave response in the resonator. In particular, the wave response at the lowest resonance mode (Helmholtz mode, pumping mode) is much greater than that at the other resonance modes, and the water surface inside the resonator rises or falls in unison. The corresponding difference of potential energy between the ocean and port sides pushes the seawater periodically into the ocean/port side through the water channel which is connected from the rear wall of the resonator to the port side. Therefore, the exchange rate of seawater across the water channel is proportional to the wave amplitude in the resonator. The shape of the resonator should be designed properly to maximize the wave response inside the resonator.

In real seas, the ocean waves are highly irregular composing of different wave heights and frequencies. However, most of the wave energy is concentrated within a certain frequency range. The shape of the resonator has to be designed so that the Helmholtz-mode natural frequency of the resonator must be precisely tuned to the peak frequency of the incident irregular waves. For tuning, the design parameters such as the radius of the semi-circular resonator and the gap width of the entrance must be selected properly. Also, the spacing of the multiple resonators may be an important design parameter too.

Recently, many researchers have used CFD simulations to study the performance of a variety of coastal structures such as breakwaters, jetties, groins, and seawalls. The flow visualization capability of the CFD tool helps to understand the flow behavior clearly near the coastal structures. Higuera *et al.* (2013) simulated diverse coastal processes such as wave interactions with an impervious rectangular column, 2D irregular wave breaking on a steep beach, 3D breaking of a solitary wave, and wave run-up on a conical island using the CFD tool OpenFOAM®. Their results indicated that OpenFOAM® with Reynolds Averaged Navier Stokes (RANS) modeling is a suitable and predictive tool for coastal engineering. The importance of the use of the RANS turbulence model in simulating wave interaction problems is growing nowadays. Ringwood (2015) used the opensource CFD tool OpenFOAM® to the simulation of numerical wave tank for testing a variety of wave energy

converters in waves. Even though OpenFOAM® is capable of serving the 3D velocity and pressure profiles, it demands a modest amount of computational resources and human effort.

In the present study, 3D numerical simulations using the opensource CFD software OpenFOAM® are performed to calculate the regular and irregular wave response in the resonator. The interFoam solver is used to solve the incompressible RANS equations, and a two-phase (water and air) flow is simulated using the volume of fluid (VOF) method. The turbulence in the fluid domain is modeled using the SST model. For waves with moderate wave steepness, the SST model performs best for wave elevation prediction along the fluid domain compared to other turbulence models (Devolder *et al.* 2017). The amplification factor in the resonator can be limited by some damping mechanisms: 1) Radiation damping, associated with energy escaped seaward from the entrance. 2) Frictional damping near the entrance. 3) Energy dissipation due to wave breaking. 4) Finite-amplitude effect of energy transfer into higher harmonics. These effects of complex nonlinear and viscous flow are revealed by the qualitative assessment of CFD. The systematic model tests are performed in a two-dimensional wave tank to validate the CFD solutions. The performance estimation of the scaled-up resonator model in real seas is evaluated in irregular waves based on the JONSWAP spectrum. The remainder of this paper is organized as follows. The details of the model experiment conditions are given in section 2. Section 3 presents a brief overview of the CFD numerical modeling and the main aspects of CFD numerical techniques. Section 4 deals with the results and discussion by comparing the numerical solutions and experimental results. Finally, conclusions are drawn in Section 5.

2. Experiments

The experiment data for the present study is taken from the model test conducted by Cho (2001). The geometry of the resonator is semi-circular with a radius (R) of 18.8 cm with an opening entrance and is connected to the port side by a water channel with a diameter (D) of 5.4 cm as shown in Fig. 2. The water channel is installed horizontally at $d=10$ cm below the still water level. The water depth (h) is fixed at 0.6 m. The amplification factor is defined as $|\eta_{ai} / A|$ and determined by wave

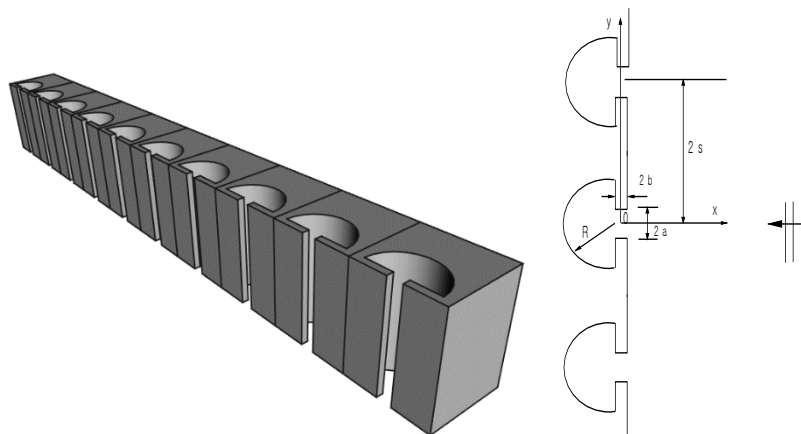


Fig. 1 Conceptual design of a seawater exchange breakwater using the Helmholtz resonator

Table 1 Details of the experiment conditions

Radius of semi-circle(R)	18.8 cm
Thickness of entrance($2b$)	1 cm
Gap width of entrance($2a$)	6,8,10 cm
Water depth(h)	60 cm
Channel diameter (D)	5.4 cm
Wave frequency (f)	0.4~1.4 Hz

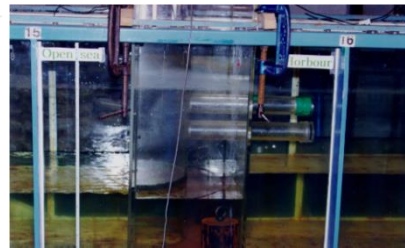
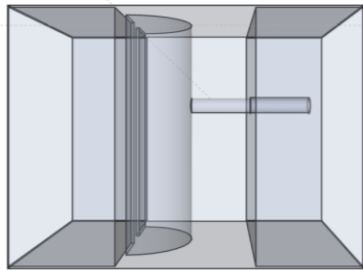
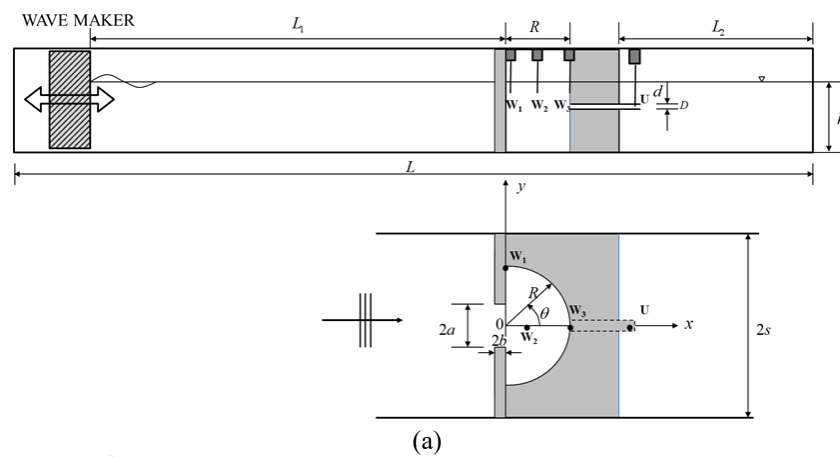


Fig. 2 Schematic view (a), 3D sketch (b), and photograph (c) of the experimental setup at a 2D wave tank

amplitudes $\eta_{ai}, (i=1,2,3)$ at three different positions (W_1, W_2, W_3). The gap widths ($2a$) of entrance are 6, 8, 10 cm, and thickness ($2b$) of the resonator 1 cm. Detailed model specifications and experimental conditions are summarized in Table 1.

3. Numerical model

The opensource CFD software OpenFOAM[®] is used to simulate the interaction of the Helmholtz

resonator with regular and irregular waves. The numerical results of regular wave simulation are then compared with the experimental data. In this section, the development of the NWT (numerical wave tank) model with a semi-circular resonator is described using OpenFOAM®. The NWT and resonator used in the present computation have the same specification as the model test conducted by Cho (2001).

3.1 RANS equations

The fluid flow is governed by incompressible RANS equations consisting of mass conservation and momentum conservation.

$$\frac{\partial u_i}{\partial x_i} = 0. \tag{1}$$

$$\frac{\partial \rho u_i}{\partial t} + \frac{\partial \rho u_i u_j}{\partial x_j} - \frac{\partial}{\partial x_i} \left[\mu_{eff} \frac{\partial u_i}{\partial x_j} \right] = -\frac{\partial p^*}{\partial x_i} + F_{b,i}. \tag{2}$$

where u_i ($i = x, y, z$) is the fluid velocities in Cartesian coordinates; p^* is the dynamic pressure. μ_{eff} the effective dynamic viscosity; $F_{b,i}$ the external gravity body force.

The interface between the water and air is tracked by the VOF method. First, the volume fraction (α) is determined by solving the following equation, which means the conservation of the mixture components along the path of a fluid parcel.

$$\frac{\partial \alpha}{\partial t} + \frac{\partial u_i \alpha}{\partial x_i} = 0. \tag{3}$$

And then a weighted average value is used to obtain the density ρ of the fluid within computational cells. As shown in Eq. (4), the effective dynamic viscosity μ_{eff} is the sum of weighted average value and an additional turbulent dynamic viscosity ($\rho \nu_t$).

$$\begin{aligned} \rho &= \alpha \rho_{water} + (1 - \alpha) \rho_{air}, \\ \mu_{eff} &= \alpha \mu_{water} + (1 - \alpha) \mu_{air} + \rho \nu_t. \end{aligned} \tag{4}$$

The discrete integration $\eta(t) = \sum_{i=0}^{N-1} \alpha_i (z_{i+1} - z_i)$ of the volume fraction (α) over a vertical line is used to obtain the free-surface elevation $\eta(t)$.

The convective and diffusive terms in incompressible RANS equations are spatially discretized using the second-order schemes, while the first-order scheme is selected for time integration. A maximum courant number of 0.65 is selected for the whole computational domain except at the water-air interface with a number of 0.45.

3.2 Turbulence model

To simulate the turbulence flow, the $k - \omega$ SST turbulence model (Menter 1994) showing good results in simulating the water waves with low wave steepness is adopted. Additional transport

equations should be solved to yield the turbulent kinematic viscosity (ν_t), which is then incorporated into the RANS equations.

The incompressible $k-\omega$ SST turbulence model for a single fluid is composed of two equations as below and formulated in OpenFOAM® ,

$$\frac{\partial k}{\partial t} + \frac{\partial u_j k}{\partial x_j} - \frac{\partial}{\partial x_j} \left[(\nu + \sigma_k \nu_t) \frac{\partial k}{\partial x_j} \right] = P_k - \beta^* \omega k. \quad (5)$$

$$\frac{\partial \omega}{\partial t} + \frac{\partial u_j \omega}{\partial x_j} - \frac{\partial}{\partial x_j} \left[(\nu + \sigma_\omega \nu_t) \frac{\partial \omega}{\partial x_j} \right] = \frac{\gamma}{\nu_t} G - \beta \omega^2 + 2(1 - F_1) \frac{\sigma_\omega}{\omega} \frac{\partial k}{\partial x_j} \frac{\partial \omega}{\partial x_j}. \quad (6)$$

with $P_k = \min(G, 10\beta^* k \omega)$, $G = \nu_t \frac{\partial u_i}{\partial x_j} \left(\frac{\partial u_i}{\partial x_j} + \frac{\partial u_j}{\partial x_i} \right)$, $\nu_t = \frac{a_1 k}{\max(a_1 \omega, SF_2)}$.

$$F_2 = \tanh \left[\left[\max \left(\frac{2\sqrt{k}}{\beta^* \omega y}, \frac{500\nu}{y^2 \omega} \right) \right]^2 \right]$$

$$F_1 = \tanh \left\{ \left\{ \min \left[\max \left(\frac{\sqrt{k}}{\beta^* \omega y}, \frac{500\nu}{y^2 \omega} \right), \frac{4\sigma_\omega k}{CD_{k\omega} y^2} \right] \right\}^4 \right\}$$

$$CD_{k\omega} = \max \left(2\rho\sigma_\omega \frac{1}{\omega} \frac{\partial k}{\partial x_i} \frac{\partial \omega}{\partial x_i}, 10^{-10} \right)$$

where k is the turbulent kinetic energy; P_k the production term of k ; ν the kinematic viscosity; ω the specific dissipation rate; S the mean strain flow rate; y is distance to the closest wall; $\beta^* = 0.09, a_1 = 0.31$; F_1 and F_2 are the blending functions. The values of $\sigma_k, \sigma_\omega, \beta$, and γ are blended using Eq. (7) in which ϕ_1 and ϕ_2 are given in Table 2.

$$\phi = F_1 \phi_1 + (1 - F_1) \phi_2 \quad (7)$$

3.3 Boundary conditions

The inlet boundary is situated on the left-most boundary of the computational domain. At the inlet boundary, waves are generated using the waves2Foam package with a relaxation length of one wavelength (λ). At the same time, a ramp time of 3s is applied. In the present study, the first-order Stokes wave is used to generate the regular waves with a wave steepness H/λ of 0.02. All the other boundaries are set to wall boundaries. At the wall boundaries, wall functions are activated to model the near-wall turbulence. The dimensionless wall distance y^+ should be between 1 and 300 according to the scalable Spalding's law wall function. As initial conditions on the wall boundaries, Dirichlet boundary condition is set for the velocity and pressure, and Neumann boundary condition is set for the volume fraction. The symmetry boundary condition is applied on the x - z plane.

Table 2 Default values of ϕ_1 and ϕ_2 for the parameters given in Eq. (7)

ϕ	σ_k	σ_ω	β	γ
ϕ_1	0.85034	0.5	0.075	0.5532
ϕ_2	1.0	0.85616	0.0828	0.4403

3.4 Computational domain

The geometry of a semi-circular resonator is modeled in FreeCAD software (see Fig. 4(a)). As the resonator is symmetric about x-z plane, only half of the resonator is used for numerical simulation. In the computational domain, the resonator is installed at the position of 3-4 wavelength away from the wavemaker and the distance (L_2) between the resonator and end wall is 2 m. The height of the computational domain including the fluid and air zone is 0.9m. Initially, a coarse background mesh is generated using the blockMesh utility. The size of the cells in this coarse mesh generation in z-direction is set to be one wave height (H). For capturing the free-surface elevation with sufficient precision, fine mesh is recreated over background mesh using snappyHexMesh utility. This fine mesh utility subdivides each cell into several cells in the z-direction. To determine the appropriate number of cells, a convergence test with different grid refinements has been conducted for an incident wave frequency of 0.9 Hz. The time history of the free surface elevation is plotted in Fig. 3. It is seen that the convergence is reached with the mesh size $\Delta z = H / 8$ when considering the accuracy and computational cost. The details of mesh refinements used in the convergence test are given in Table 3.

After selection of cell size Δz of the z-direction, the cell size ($\Delta x, \Delta y$) in the other two directions is determined automatically with an aspect ratio of 2. The fine mesh is applied in the resonator where large wave elevation occurs. Also, domain near the water channel is discretized using the fine mesh to capture the flow variations efficiently. Fig. 4 shows the geometric model used in CFD calculation, mesh distribution in the whole computational domain, and fine mesh near the resonator.

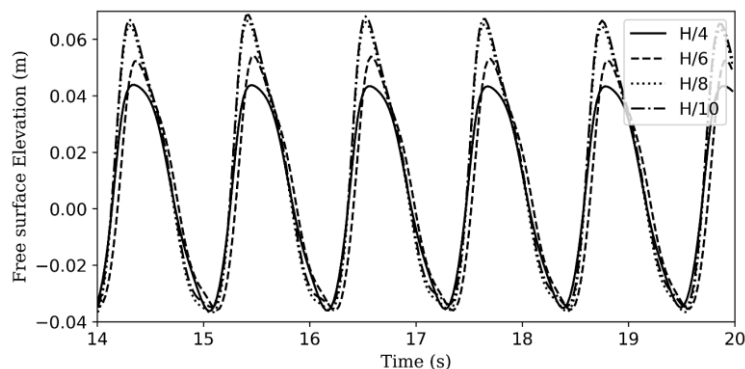
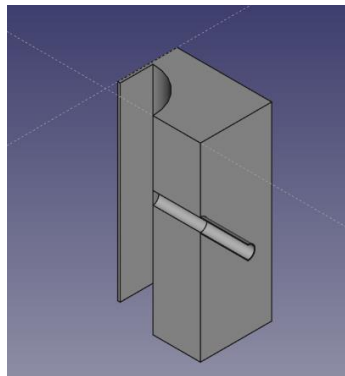


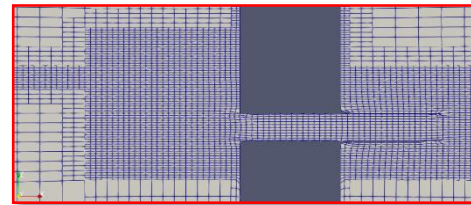
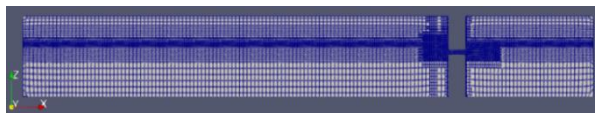
Fig. 3 Time history of surface elevation at the position W_3 in the resonator for different mesh refinements ($f = 0.9$ Hz)

Table 3 Number of grid cells for each mesh refinements

Case	Δz	Cells
1	$H/4$	53528
2	$H/6$	195262
3	$H/8$	298170
4	$H/10$	701912



(a)



(b)

Fig. 4 Geometric model of the resonator with a water channel (a) and its computational domain and mesh details (b)

4. Results and discussion

4.1 Regular waves

In this section, the numerical results from OpenFOAM simulations are compared with the experimental data in regular waves. First, the time-history of the free-surface elevation ($\eta_i(t)/A$) at three different positions (W_1, W_2, W_3) in the resonator is shown in Fig. 5 for three different frequencies 0.6 Hz, 0.9 Hz, and 1.1 Hz. When comparing the time history for three different frequencies, nonlinear behavior like wave distortion is predominant at the high-frequency.

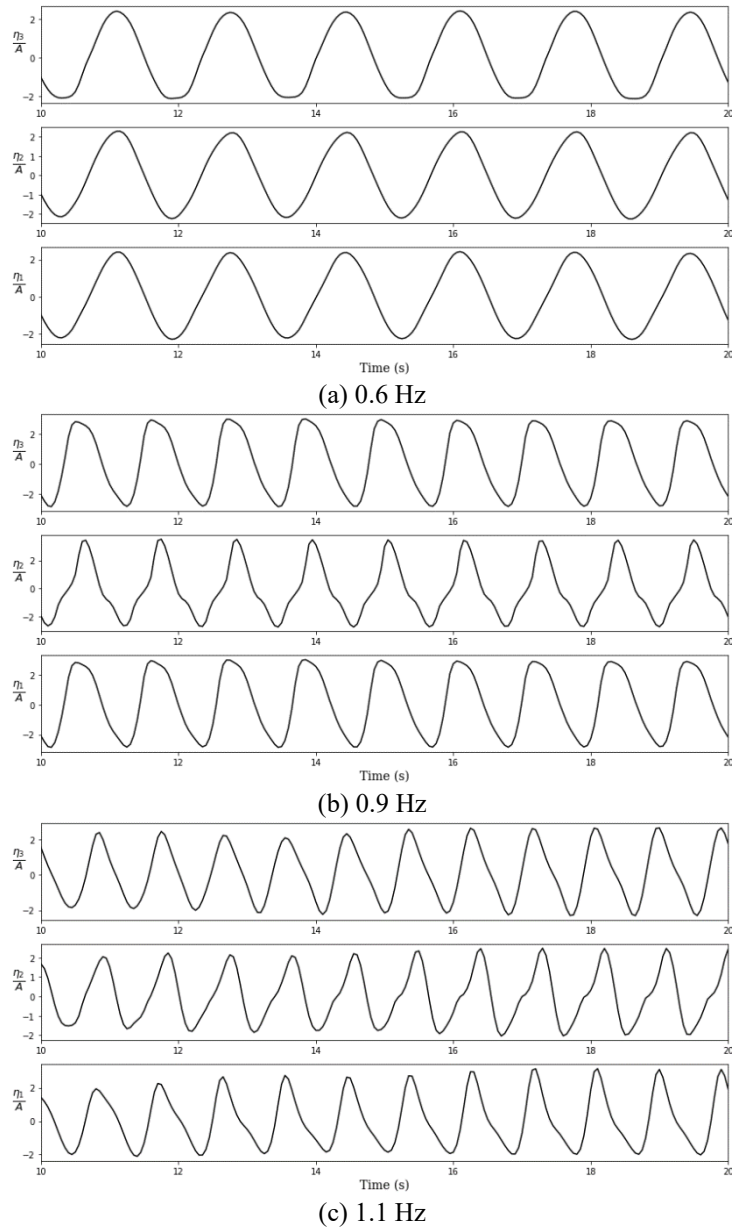


Fig. 5 Time history of free-surface elevation at three different positions (W_1, W_2, W_3) for different wave frequencies $f = 0.6, 0.9, 1.1$ Hz

The amplification factor ($|\eta_{ai} / A|$) between the CFD solutions and experimental results is compared as a function of wave frequencies in Fig. 6. In general, the CFD solutions are in good agreement with the experimental results. But, some quantitative differences appear near resonance frequency. From Fig. 6, it is shown that the amplification factor has a similar value at resonance frequency regardless of the position. When the lowest-mode (Helmholtz mode) resonance occurs,

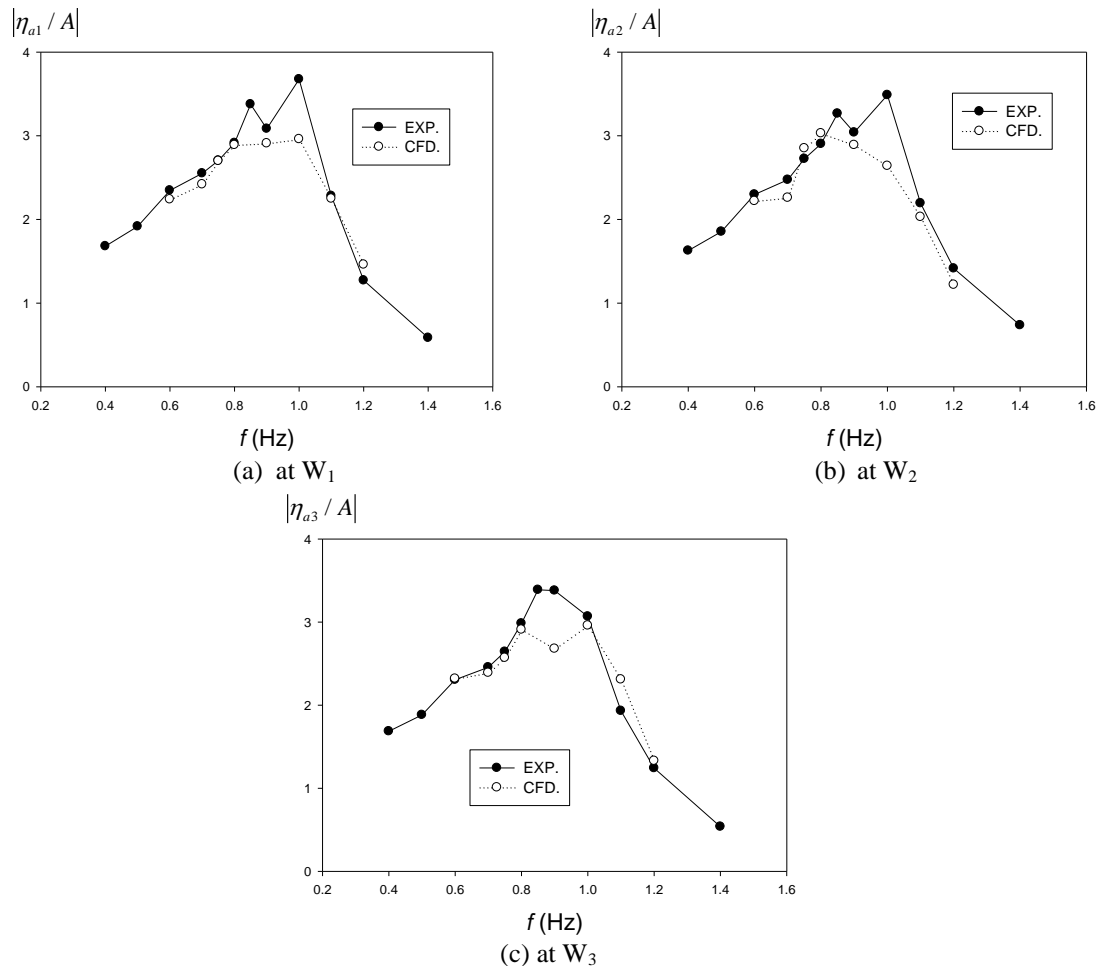


Fig. 6 Comparison of amplification factor between OpenFOAM numerical solutions and experimental results at different locations (W_1, W_2, W_3) in the resonator for $R=18.8$ cm, $2a=10$ cm and $2b=1$ cm

the free-surface elevation in the resonator rises and falls uniformly in unison. It can be also proved by the fact that the wave elevations in the resonator oscillate in phase regardless of the position of the wave probe as shown in Fig. 5.

Fig. 7 shows the horizontal flow velocity ($U(t)$) at the center of a water channel to quantify the seawater exchange capability using the Helmholtz resonator. The time history of the horizontal flow velocity for three different wave frequencies (0.6, 0.9, 1.1 Hz) is displayed. At a wave with a relative low-frequency (0.6 Hz), the seawater with a higher flow velocity passes back and forth having equal amplitude for both directions. It implies that the seawater is exchanged and mixed effectively through a water channel. On the other hand, in the case of the highest-frequency wave (1.1 Hz), the flow velocity in the direction from the ocean to the port side is more dominant than that in the opposite direction. But the magnitude of flow velocity is much smaller when being compared to the low-frequency wave. From these facts, it can be said that the present resonator model can exchange the seawater more effectively at the low-frequency wave region. Also, by comparing the time

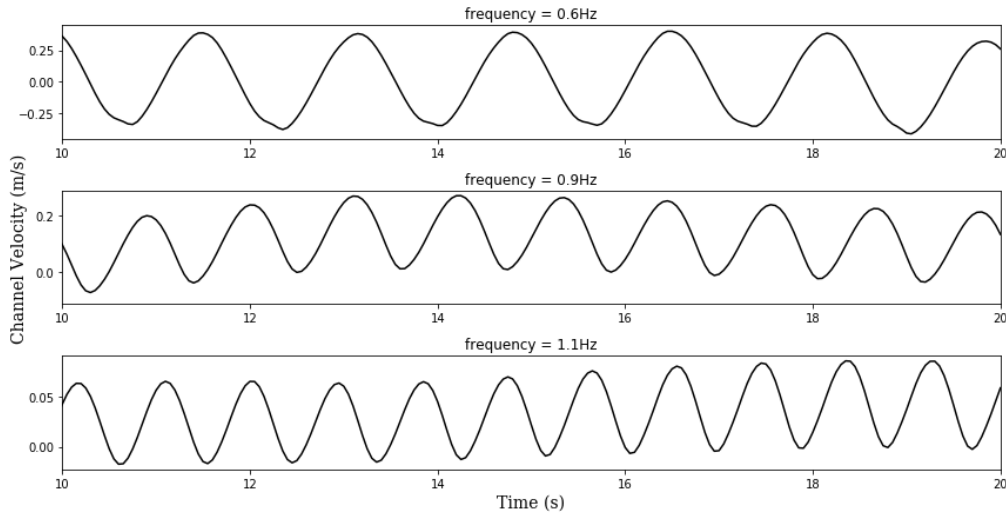


Fig. 7 Time history of channel flow velocity through a water channel at different wave frequencies

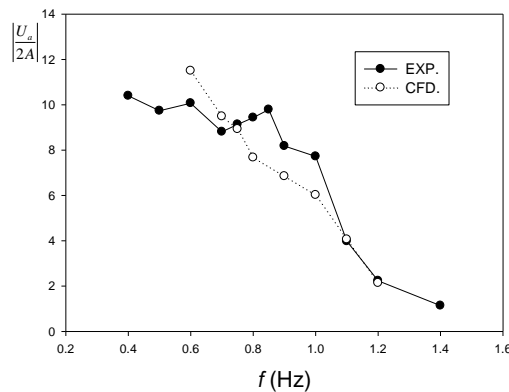


Fig. 8 Comparison of channel flow velocity against wave frequencies between OpenFOAM numerical solutions and experimental results for $R=18.8$ cm, $2a=10$ cm, and $2b=1$ cm

histories of free surface elevation at the wall (Fig. 5) and time histories of channel flow velocity (Fig. 7) for different frequencies, we can draw some conclusions. For lowest-frequency wave (0.6 Hz), the channel flow velocity is well correlated to the free-surface elevation in the resonator and as the frequency of the wave increases the phase difference between the channel flow velocity and the free surface elevation increases.

Fig. 8 shows the comparison of the horizontal flow velocity between the CFD solutions and experimental results. Here, the filled circles denote the experimental data. The channel flow velocity shows a decreasing trend with the increase of wave frequency. As described in Fig. 7, when waves with the lower-frequency propagate to the resonator, the seawater exchange through a water channel is more dominated. It is because the resonator needs sufficient time in pushing the amount of seawater in one direction effectively under reciprocating flow through a water channel. Overall, there exists a satisfactory agreement between the OpenFOAM® results and experimental data.

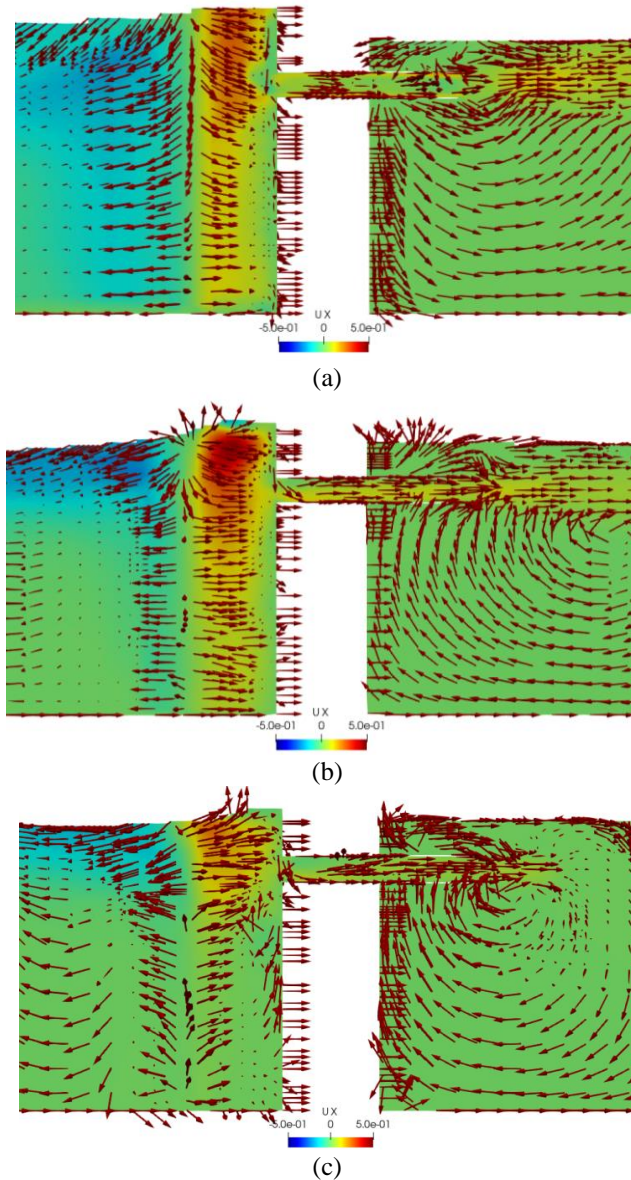


Fig. 9 Flow visualization near the resonator and water channel for frequency 0.6Hz (a) 0.9Hz (b) 1.1Hz (c)

Using post-processing of the OpenFOAM[®] solution, we can visualize the flow velocity field at the cross-sectional (x - z) plane as shown in Fig. 9. Three wave frequencies are chosen for this visualization. The snapshots are taken at an instant when the free-surface elevation inside the resonator is at maximum. In the figure, the color of the surface represents the magnitude of the particle velocity in x -direction in the wave field. A blue-red color scheme is used herein, in which red color means the large positive particle velocity, whereas blue color indicates large negative velocity. The red arrows in the figure depict the velocity vector at the respective points. From this plot, we can verify the direction and magnitude of the velocity at different locations.

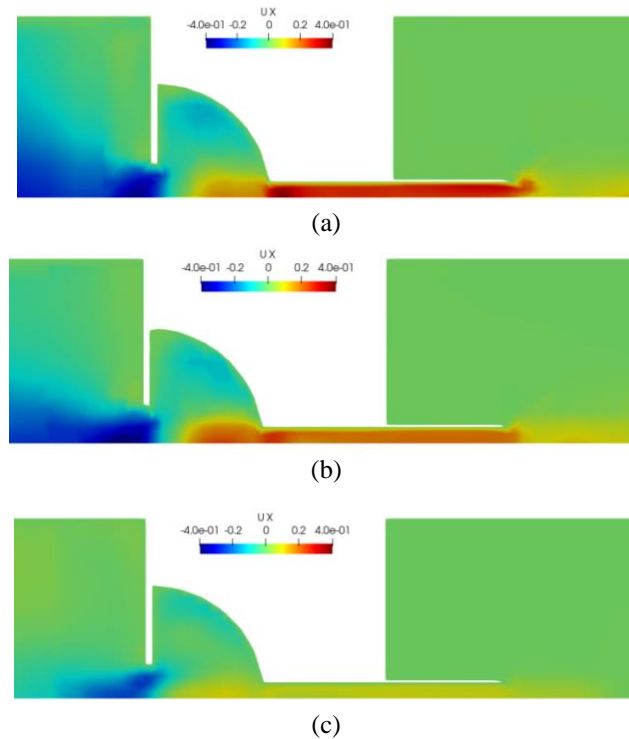


Fig. 10 Flow visualization on a horizontal plane passing through the center of the channel for frequency 0.6Hz (a) 0.9Hz (b) 1.1Hz (c)

Furthermore, the flow velocity in the x-direction inside the channel is visualized on a horizontal (x-y) plane. The visualization plots for different frequencies are given in Fig. 10. Same as Fig. 9, the blue-red color scheme is used for the representation of the magnitude of the flow velocity. The snapshots are taken at a time instant when the channel flow velocity is maximum. As it is obvious from the time histories of the channel velocity, at low-frequency incident wave (0.6 Hz) the channel flow velocity is largest compared to the other two cases. This visualization confirms that the seawater exchange performs best in the low-frequency incident wave region.

Fig. 11 shows the comparison of the amplification factor at the position W_1 against the change of the gap width of the entrance from the model experiments. From the plot it is obvious that less wave energy radiates out to the seaward with decreasing of the gap width of the entrance. Thus, wave response in the resonator becomes larger with the reduction of radiation damping. However, in the experimental results, the contrary trend is shown. It can be explained that the experiments are conducted in the long-wave range compared to the resonator size. As a result, the wider the gap width, the more the incident wave energy into the resonator than the radiated wave.

Fig. 12 plots the channel flow velocity divided by wave height against the gap width of the entrance from the model experiments. It is expected that the magnitude of flow velocity is proportional to the amplification factor drawn in Fig. 6. However, it is shown that the channel flow velocity is too exaggerated in the low-frequency region compared to the curve of the amplification factor. The channel flow shows a reciprocating motion with the same frequency as the wave response in the resonator. When the channel flow direction changes, a new fluid flow with a reversed direction

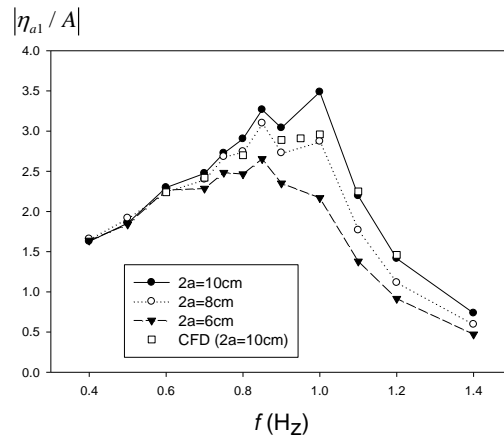


Fig. 11 Experimental results of amplification factor at the W_1 position as a function of the gap width of the entrance for $R=18.8$ cm and $2b=1$ cm

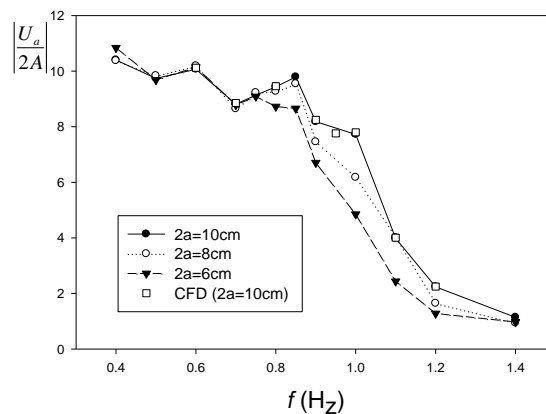


Fig. 12 Experimental results of flow velocity at the water channel as a function of the gap width of the entrance for $R=18.8$ cm and $2b=1$ cm

is formed in the channel while overcoming the already existed flow. Therefore, it is difficult to get the meaningful channel flow velocity under the short periodic wave motion. Consequently, the flow velocity at the low-frequency is greater than that at the high-frequency. To overcome these demerits, it is necessary to install a check valve in the water channel to make a one-way flow be possible.

4.2 Irregular waves

To investigate the performance of a seawater exchange breakwater using the Helmholtz resonator in the real seas, CFD simulations have been conducted for a prototype resonator (scale ratio: $S=18.6$) in irregular waves. The radius of the resonator (R) is 3.5 m. The gap width of the entrance ($2a$) is 2 m and its thickness ($2b$) is 0.4 m. The water channel has a diameter (D) of 1m and is positioned at 2 m below the free surface. The water depth is 30 m and the total length (L) of NWT is set to be 12 m. In the process of simulation, the free surface elevation is collected at three different positions

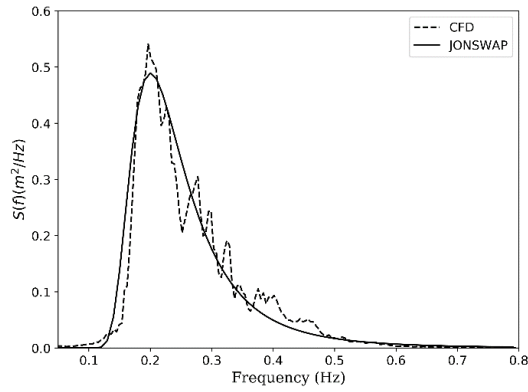
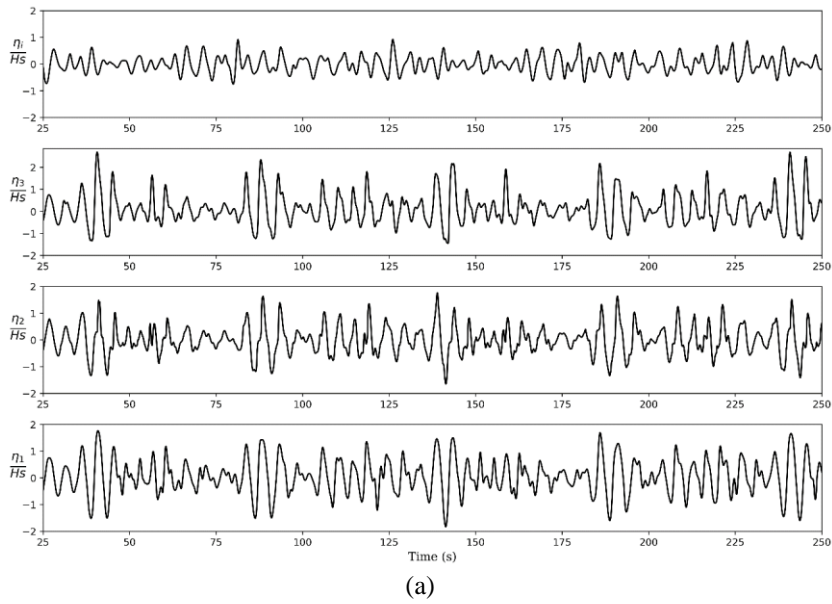
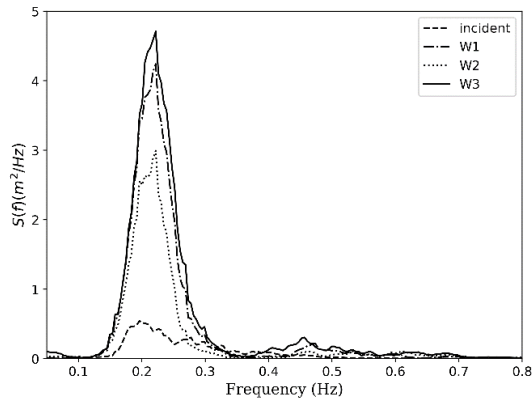


Fig. 13 Comparison of target and generated wave spectrum



(a)



(b)

Fig. 14 Time history of both the incident wave and surface elevations in a resonator (a), and its wave spectra (b)

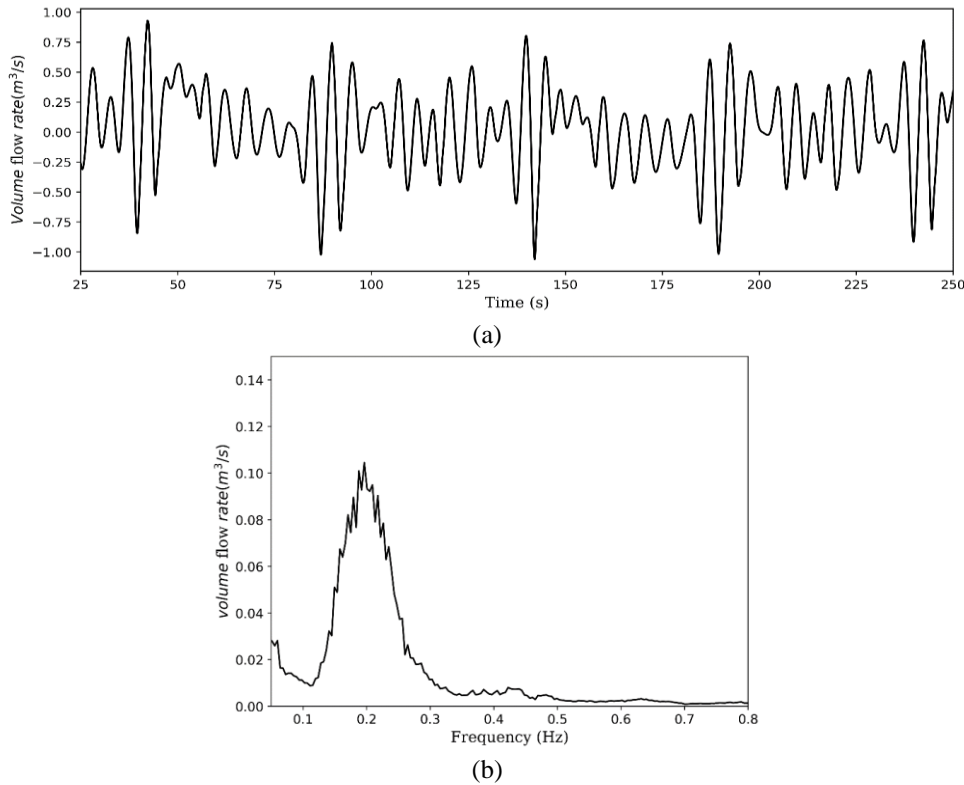


Fig. 15 Time history of volume flow rate (a) in the water channel and its amplitude spectra (b)

(W_1, W_2, W_3) inside the resonator, and the volume flow rate ($Q = \int_A U dA$) of unit m^3/s is obtained at the center of a water channel.

Irregular waves based on JONSWAP spectrum with the significant period and height ($T_s = 5\text{s}$, $H_s = 1\text{m}$, $\gamma = 1$) are generated using the toolbox waves2Foam. The peak period of the target spectrum is close to the scale-up value ($T_p = \sqrt{S}T_m = 4.8\text{s}$) of the Helmholtz resonance period ($T_m = 1.1\text{s}$) shown in Fig. 6. In spatial discretization of the computational domain, the minimum cell size of $H_s/8$ is used at the interface. All other simulation settings are the same as that of regular wave simulation. Fig. 13 shows the comparison between the target spectrum and generated spectrum. The total number of cells in the domain is 453,717. The simulation time is 250s which takes 104 hours to complete on intel® Core™ i7-2600k CPU with 8 processors.

Fig. 14(a) shows the time histories of the incident wave η_i and surface elevations η_i , $i = 1, 2, 3$ at three different locations (W_1, W_2, W_3). The surface elevations in a resonator are non-dimensionalized with significant wave height H_s . From this figure, it is obvious that the high wave responses in the time series are always in phase. It means that the high wave elevation amplified by resonance rises and falls in unison. Fig. 14(b) shows the energy spectra of wave elevations at the different positions in the resonator along with the incident wave spectra. From this figure, we can assess there is significant amplification of the wave energy in the resonator due to the Helmholtz

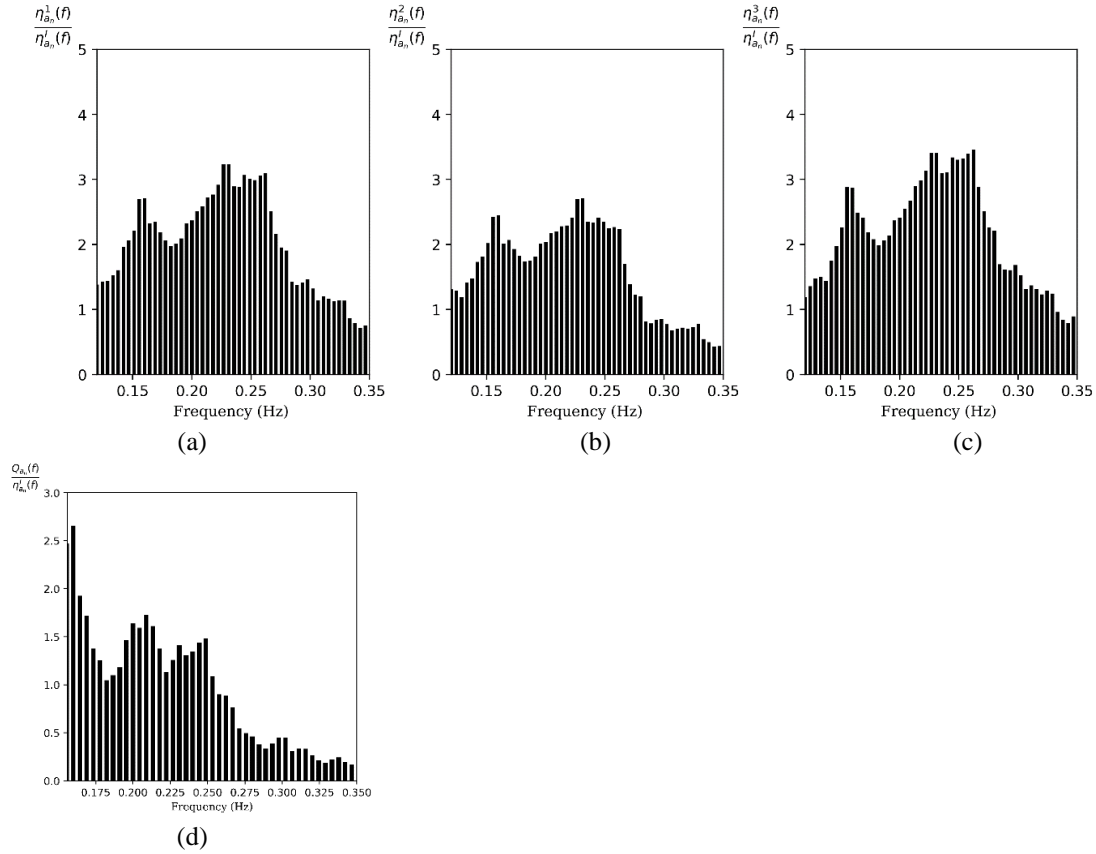


Fig. 16 Amplification factor of surface elevations in a resonator and volume flow rate through a water channel from irregular wave test

resonance. And the difference of the wave energy exists according to the position in the resonator, which means the spatial non-uniformity of the wave displacement due to the presence of short-period waves among the irregular waves. Overall, the Helmholtz resonator is effective in increasing wave elevation inside the resonator and assures spatial uniformity even in irregular waves.

The volume flow rate through the water channel is an important parameter that quantifies the seawater exchange capability of the developed seawater exchange breakwater. Fig. 15(a) shows the time history of volume flow rate $Q(t)$ passing through the water channel. From the time series of volume flow rate, it is seen that the flow happens periodically in both directions and seawater exchanges between the ocean and port side with a maximum value of approximately $1 \text{ m}^3/\text{s}$. Fig. 15(b) shows the amplitude spectrum of volume flow rate. The peak frequency of the spectrum coincides with the frequency of the Helmholtz resonance exactly.

The amplification factors for surface elevations inside the resonator can be also obtained in irregular waves simulation. The wave elevation of irregular waves is composed of the sum of a large number of regular wave components $\eta(t) = \sum_{n=1}^N \eta_{a_n} \cos(k_n x - 2\pi f_n t + \varepsilon_n)$, where amplitudes η_{a_n} can be obtained by a Fourier analysis of the time signals. The amplification factor can be calculated as follows by dividing the discrete amplitude spectrums $\eta_{a_n}^i(f_n), i=1,2,3$ of surface elevations inside

the resonator by the amplitude spectrum $\eta_{a_n}^l(f_n)$ of the incident wave. The resulting amplitude factors of surface elevations at three different locations (W1, W2, W3) are plotted in Figs. 16(a)-16(c). The peaks of the amplification factor curve are about 3.5 and peak frequencies are observed around 0.25 Hz, which agrees with the natural frequency of Helmholtz resonator. Even though the direct comparison to a small-scaled model is impossible, the present results with a prototype show the same trend as observed in Fig. 16. In the same manner, we can obtain the amplification factor of the volume flow rate passing through a water channel by dividing the amplitude spectrum $Q_{a_n}(f_n)$ of the volume flow rate by the amplitude spectrum $\eta_{a_n}^l(f_n)$ of the incident wave. The peak value of the amplification factor is about 2.66 which is observed at the frequency of 0.16 Hz. It is shown that the seawater exchange capability prevails in the low-frequency region.

5. Conclusions

The opensource CFD software OpenFOAM® has been used to simulate the numerical experiment of the Helmholtz resonator with a water channel. The water-air interface is tackled by the VOF method and turbulent flow in the fluid domain is modeled by $k-\omega$ SST model. The RANS equations are solved by interFoam solver of the OpenFOAM®. The present numerical results are compared with a series of regular wave experiments conducted by authors in a 2-D wave tank, which shows reasonable agreement between them. Consequently, the proposed numerical model is proved to be a good predictive tool for studying the performance of the seawater exchange breakwater.

To study the performance of seawater exchange rate in the real seas, CFD simulations are extended to irregular waves with a prototype model. The wave energy spectrum at different positions in the resonator is calculated under the irregular incident waves based on the JONSWAP spectrum. On the contrary to regular waves, a spatial non-uniformity of the surface elevation inside the resonator is observed due to the presence of short-period waves among the irregular waves. However, the relatively high waves generated by the Helmholtz resonance follow the spatial uniformity in the resonator. The volume flow rate through the water channel is an important index in quantifying the seawater exchange capability of the present model. The numerical results show that seawater exchange happens periodically in both directions with a maximum volume flow rate of 1.06 m³/s in negative x-direction and 0.93 m³/s in positive x-direction. Using the flow visualization, the characteristics of the periodic flow pattern around the resonator and water channel are emphasized.

Through the systematic numerical and experimental study, it is concluded that the seawater exchange capability is enhanced greatly in the low-frequency wave region, where the Helmholtz mode resonance frequency belongs. The Helmholtz resonator is effective in increasing wave elevation inside the resonator and gives a spatial uniformity of wave displacement even in irregular waves. In the future, the optimum vertical position and horizontal length of the channel will be predicted using the present numerical model.

Acknowledgements

This research was supported by the Basic Science Research Program through the National Research Foundation of Korea (NRF) funded by the Ministry of Education (NRF-2017R1D1A1B04035231), South Korea.

References

- Cho, I.H. (2001), "Performance evaluation of seawater exchanging breakwater using Helmholtz resonator", *J. Korean Soc. Coast. Ocean Engineers*, **13**(2), 89-99. (In Korean)
- Devolder, B., Rauwoens, P. and Troch, P. (2017), "Application of a buoyancy-modified k- ω SST turbulence model to simulate wave run-up around a monopile subjected to regular waves using OpenFOAM®", *Coast. Eng.*, **125**, 81-94. <https://doi.org/10.1016/j.coastaleng.2017.04.004>
- Higuera, P., Lara, J.L. and Losada, I.J. (2013), "Realistic wave generation and active wave absorption for Navier-Stokes models. Application to OpenFOAM®", *Coast. Eng.*, **71**, 102-118. <https://doi.org/10.1016/j.coastaleng.2012.07.002>.
- Higuera, P., Lara, J.L. and Losada, I.J. (2013), "Simulating coastal engineering processes with OpenFOAM®", *Coast. Eng.*, **71**, 119-134. <https://doi.org/10.1016/j.coastaleng.2012.06.002>.
- Hirt, C.W. and Nichols, B.D. (1981), "Volume of fluid (VOF) method for the dynamics of free boundaries", *J. Comput. Phys.*, **39**(1), 201-225. [https://doi.org/10.1016/0021-9991\(81\)90145-5](https://doi.org/10.1016/0021-9991(81)90145-5).
- Jacobsen, N.G., Fuhrman, D.R. and Fredsøe, J. (2012), "A wave generation toolbox for the open-source CFD library: OpenFoam®", *Int. J. Numer. Meth. Fl.*, **70**(9), 1073-1088. <https://doi.org/10.1002/flid.2726>.
- Kim, K.H., Seo, H. and Kobayashi, N. (2011), "Field assessment of seawater exchange breakwater", *J. Waterwa. Port Coast. Ocean Eng.*, **137**(3), 146-149. [https://doi.org/10.1061/\(asce\)ww.1943-5460.0000058](https://doi.org/10.1061/(asce)ww.1943-5460.0000058).
- Lee, C. and Lee, D.S. (2003), "Water surface resonance in the L-shaped channel of seawater exchange breakwater", *Ocean Eng.*, **30**(18), 2423-2436. [https://doi.org/10.1016/S0029-8018\(03\)00102-1](https://doi.org/10.1016/S0029-8018(03)00102-1).
- Lee, D.S., Park, W.S. and Kobayashi, N. (1995), "Circular channel breakwater to reduce wave overtopping and allow water exchange", *Proceedings of the 24th International Conference on Coastal Engineering*, Kobe, Japan, October. <https://doi.org/10.1061/9780784400890.100>.
- Menter, F.R. (1994), "Two-equation eddy-viscosity turbulence models for engineering applications", *AIAA J.*, **32**(8), 1598-1605. <https://doi.org/10.2514/3.12149>.
- OpenFOAM® v1912 (19 12), <https://www.OpenFOAM®.com/>
- Ringwood, J.V. (2015), "Implementation of an OpenFOAM Numerical Wave Tank for Wave Energy Experiments", *Proceedings of the 11th European Wave and Tidal Energy Conference*, Nantes, France, September.
- Van Der Meer, J.W. (1995), Conceptual Design of Rubble Mound Breakwaters, 221-315. https://doi.org/10.1142/9789812797582_0005.